The SPOrt Project: Cosmological and Astrophysical Goals

R. Fabbri*, S. Cortiglioni†, S. Cecchini†, M. Orsini†‡, E. Carretti‡‡,
G. Boella¶, G. Sironi¶, J. Monari§, A. Orfei§, R. Tascone§§, U. Pisani§*,
K.W. Ng||, L. Nicastro**, L. Popa††, I.A. Strukov‡‡, M.V. Sazhin¶¶

*Dipartimento di Fisica, Università di Firenze, Via S. Marta 3, I-50139 Firenze, Italy
†I.Te.S.R.E./CNR, Via P. Gobetti 101, I-40129 Bologna, Italy
‡Dipartimento di Astronomia, Università di Bologna, Via Zamboni 33, I-40126 Bologna
¶Dipartimento di Fisica, Università di Milano, Via Celoria 16, I-20133 Milano, Italy
§I.R.A./CNR VLBI Radioastronomical Station of Medicina, Via P. Gobetti 101, I-40129 Bologna, Italy
§§CESPA/CNR c/o Dpt. Elettronica Politecnico di Torino, c.so Duca degli Abruzzi 24, 10129 Torino, Italy
§*Dpt. Elettronica Politecnico di Torino, c.so Duca degli Abruzzi 24, 10129 Torino, Italy
||Institute of Physics, Academia Sinica, Taipei, Taiwan 11529, R.O.C.
**I.F.C.A.I./CNR, Via U. La Malfa 153, I-90146 Palermo, Italy
††Institute of Space Sciences, R-76900 Bucharest-Magurele, Romania
‡‡Space Research Institute (IKI), Profsojuznaja ul. 84/32, Moscow 117810, Russia
¶¶Schternberg Astronomical Institute, Moscow State University, Moscow 119899, Russia

Abstract. We present the cosmological and astrophysical objectives of the SPOrt mission, which is scheduled for flying on the International Space Station (ISS) in the year 2002 with the purpose of measuring the diffuse sky polarized radiation in the microwave region. We discuss the problem of disentangling the cosmic background polarized signal from the Galactic foregrounds.

INTRODUCTION

SPOrt is an experiment selected by the European Space Agency for the International Space Station and intended to measure the linear polarization of the diffuse sky radiation at an angular resolution of 7° in the 20–90 GHz frequency range. Although it was originally planned to measure the polarized Galactic background, its present design will possibly allow the detection of the polarization of the Cosmic Background Radiation (CBR). Differing from the other planned space experiments (MAP (1) and PLANCK (2)), it is specifically designed for a clean measurement of the Stokes parameters Q and U, with no significant limitation arising from spurious polarization. The instrumental design is presented in a companion paper in this volume (3). Here we discuss the experiment's expected performance (sensitivity and sky coverage) and the capability to detect and discriminate between the various contributions to the sky polarized background. Generally speaking, an experiment sensitivity derived from instrumental noise alone may not provide an accurate evaluation of the effective sensitivity for the Stokes parameters of CBR (or the other backgrounds). This point will be considered in this paper, deriving in particular a reliable estimate of SPOrt effective sensitivity to CBR. According to our analysis, taking into account both the present experimental knowledge and the theoretical models, we can realistically expect to obtain the following results from SPOrt:

- High-accuracy, low-resolution maps of Galactic synchrotron at the lowest frequencies,
- discrimination of low temperature dust in our Galaxy,
- and last but not least, the detection of CBR polarization at 60–90 GHz if the cosmic medium underwent a secondary ionization and the reheating optical depth was not too weak, say $\tau_{\rm rh} \gtrsim 0.1$.

TABLE 1. SPOrt expected performance.

ν (GHz)	$P_{\rm pix}$ **(ave)**[a] (μK)	$P_{\rm rms}$ **(FS)**[b] (μK)	$P_{\rm rms}$ **(GC)**[c] (μK)
22	13.4	0.52	0.64
32	13.8	0.54	0.66
60	14.7	0.57	0.70
90	16.8	0.65	0.81

[a] Computed for 50% efficiency and 10% frequency bandwidth.
[b] Full sky (FS) coverage is 81.7% of 4π sr, including 662 pixels.
[c] Galactic cut (GC) excludes a $\pm 20^\circ$ belt about the Galactic plane, retaining 445 pixels.

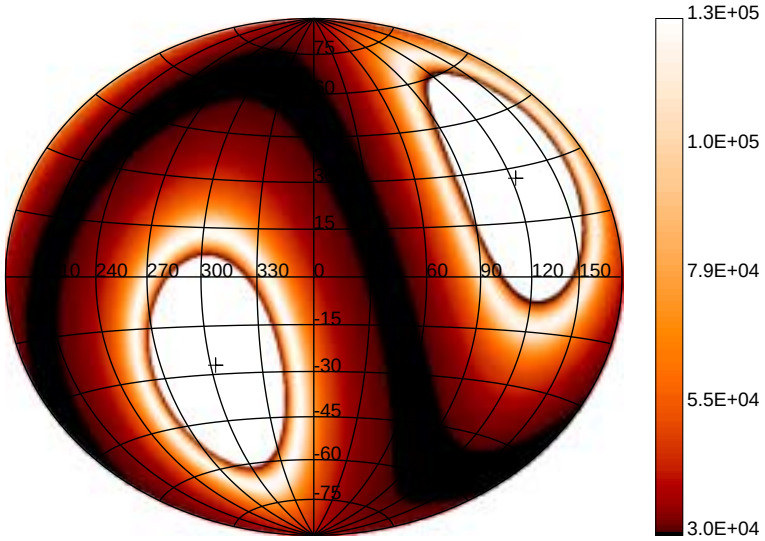

FIGURE 1. Galactic projection of the SPOrt sky coverage. Exposure times in seconds are shown on the right bar. Regions around the celestial poles (marked) are uncovered because of pointing constraints.

SPOrt'S CHARACTERISTICS

The expected performance for each of the frequency channels (22, 32, 60 and 90 GHz) is summarized in Table 1. Column 2 in the Table gives the mean sensitivity per 7° pixel, expressed in terms of the total polarized intensity $P = (Q^2 + U^2)^{\frac{1}{2}}$. The integration time per pixel will depend on sky coordinates, ranging from 29.7 Kilosec (for low values of declination δ) to 128.5 Kilosec (for the largest values of $|\delta|$ compatible with the orbit of ISS). The reported $P_{\rm rms}$ are computed using actual integration times and the noise-equivalent temperatures reported by (3), the spurious polarization limit being lower than noise. They also include a 50% efficiency factor. Column 3 in the Table gives the full-sky sensitivity for the total sky coverage, which includes 662 pixels and is shown in Figure 1. The last column gives the sensitivity after subtraction of a Galactic plane belt of $\pm 20^\circ$. Clearly the pixel sensitivity $P_{\rm pix}$ is intermediate between the expected sensitivities of MAP (1) and PLANCK (2). However the beamwidth is much larger here, so that the full-sky $P_{\rm rms}$ cannot be better than 0.5–0.6 μK for each channel.

THE EXPECTED SCENARIO FOR GALACTIC FOREGROUNDS

Generally speaking, both the Galactic and the extragalactic background should be considered as foregrounds with respect to CBR. However the extragalactic source contribution should be negligible at our resolution. Galactic emission includes three contributions related to different physical processes, namely, synchrotron produced by relativistic electrons moving in the Galactic magnetic field, free-free (Bremsstrahlung) arising from interaction between free electrons and ions in a plasma, and dust emission of thermal origin.

The frequency dependence of synchrotron emission is usually approximated by a power law in terms of antenna temperature (but the spectral index depends on spatial position and also changes with frequency),

$$T_{\rm S} \propto \nu^S, \quad S = -(2.6 \div 3.2). \tag{1}$$

Large sky coverage surveys are only available at low frequencies (4–6), and extrapolations to the microwave region can be made through Eq. (1). From the 1.4 GHz linearly polarized galactic emission survey of Brouw and Spoelstra (4) with $S = -3.2$ we get $T_{\rm S}(30\ {\rm GHz}) \simeq 40\ \mu$K. Constraints on the rms fluctuation of the emission are set from CBR anisotropy measurements. From COBE–DMR (7–8) we have a 7° fluctuation $\delta T_{\rm S} \lesssim 7\ \mu$K at 53 GHz. From the Tenerife experiment Davies and Wilkinson (9) are able to derive a 5°–8° fluctuation $\delta T_{\rm Galactic} \lesssim 43\ \mu$K at 10 GHz in the Northern low emissivity region, so that we can extrapolate $\delta T_{\rm S}(30\ {\rm GHz}) \lesssim 2\ \mu$K; this limit however is not expected to hold over most of the sky. The intrinsic polarization degree $\Pi = P/I$ can be easily predicted for synchrotron,

$$\Pi_{\rm S} = (3S+3)/(3S+1), \tag{2}$$

so that values as high as $\simeq 75\%$ are expected. However misalignment and smearing effects should reduce the measurable $\Pi_{\rm S}$, so that at 7° a better estimate is probably $\lesssim 30\%$.

Free-free emission seems to be the main source of foreground at $\nu \gtrsim 20$ GHz for CBR *anisotropy* measurements. Its spectral dependence is accurately described by a power law rather insensitive of spatial position and frequency

$$T_{\rm FF} \propto \nu^F, \quad F \simeq -2.15. \tag{3}$$

From COBE–DMR Kogut et al. (7–8) it can be obtained $\delta T_{\rm FF}(53\ {\rm GHz}) = 7 \pm 2\ \mu$K at $|b| > 20°$ and some correlation with dust, i.e., with DIRBE. From Tenerife the extrapolated limit $\delta T_{\rm FF}(30\ {\rm GHz}) \lesssim 4\ \mu$K is derived (9), which again should not be considered as typical for the whole sky. Oliveira et al. (10) find DIRBE–Saskatoon cross-correlations and derive $\delta T_{\rm FF}(40\ {\rm GHz}) = 17 \pm 10\ \mu$K at 1°. Free-free emission can be polarized via Thomson scattering within optically thick plasma regions (11). At microwave wavelengths HII regions are to be considered optically thin; thus estimating an $\Pi_{\rm FF} \lesssim 5\%$ is probably a conservative upper limit.

Dust emission is modelled with power law with index 1.5÷2, or with a greybody, or following Wright et al. (12), with a mixture of two greybodies with emissivities $\simeq 2$,

$$T_{\rm D} \propto \nu^{D-2}\left[B_\nu(20.4\ {\rm K}) + 6.7 \cdot B_\nu(4.77\ {\rm K})\right], \quad D \simeq 2. \tag{4}$$

This emission is obviously better known at high frequencies. IRAS and DIRBE data at $\nu \geq 10^3$ GHz are usually utilized for templates or cross-correlations (7,10) rather than extrapolations to the microwave region. From COBE–DMR (8) we have $\delta T_{\rm D}(53\ {\rm GHz}) = 2.7 \pm 1.3\ \mu$K, which implies $\delta T_{\rm D}(100\ {\rm GHz}) \sim 10\ \mu$K. Dust emission can be polarized (provided dust grains are aligned by the Galactic magnetic field), probably to a level of $\sim 10\%$ (13). Sethi et al. (14) have recently provided a detailed modelling for the angular spectrum of polarized dust emission. Using the Leiden–Dwingloo HI maps and a relation between dust optical depth and HI column density, they compute the microwave emission over the sky, and from a model of spheroidal silicate-graphite grains derive an intrinsic $\Pi_{\rm D}$ of 30%. Finally modelling the Galactic magnetic field they compute the polarization reduction factor. From their results we derive the estimate $P_{\rm D} \simeq 0.05\ \mu$K at $\nu \simeq 100$ GHz on scales of 7°. This is considerably lower than the estimate from COBE–DMR with $\Pi_{\rm D} = 10\%$. The discrepancy is indicative of the existing uncertainties on dust polarized emission at microwave frequencies.

In Fig. 2 we provide estimates for the Galactic foregrounds compared with SPOrt sensitivity limits. Clearly synchrotron emission can easily be measured at the lowest frequencies. Free-free emission, on the other hand, is not expected to dominate at any frequency in the 20–90 GHz range.

CBR POLARIZATION

Present experimental status

In the last two decades published results on CBR polarization show an improvement in sensitivity of roughly one order of magnitude, which was not sufficient to give a positive detection. Table 2 reports the available

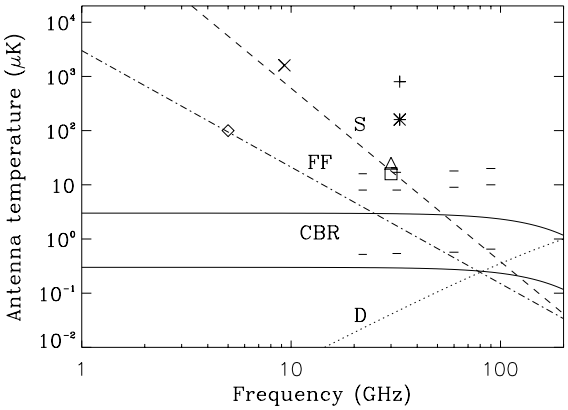

FIGURE 2. Expected Galactic foregrounds in the microwave region. Synchrotron (S) and free-free (FF) polarized emissions are normalized to 18 μK and 2 μK, respectively, at 30 GHz, and dust (D) to 1 μK at 100 GHz. Also reported are the CBR signal normalized to 1% and 10% of anisotropy, the experimental upper limits quoted in Table 2 and the SPOrt sensitivities. For each frequency channel we give the maximum and minimum $P_{\rm pix}$, and $P_{\rm rms}$.

upper limits on $\Pi_{\rm rms}$, the rms polarization degree at the corresponding scales α for the sky coverages given in the 4-th column. The most stringent limit is 16 μK on a scale of $1\overset{\circ}{.}4$, for a fairly wide window about the North Celestial Pole (21). It should be noted that the upper limits on the full sky $\Pi_{\rm rms}$ would be even weaker than those reported in Table 2.

As we shall discuss in the next Section, the goal must be a sensitivity better than a few μK at $\alpha < 1^\circ$ and better than a few tenths of μK at $\alpha > 1^\circ$. Several experiments are in preparation or in the course of execution (22,23,11) at angular scales ranging from a few arcminutes to 14°. The best prospects for positive detection, however, are linked to space experiments (1–3).

Theoretical predictions

The main sources of CBR polarization are the metric perturbations of spacetime, which include scalar (density), vector (velocity) and tensor (gravitational) waves; such perturbations directly generate anisotropy, and polarization is thereby excited by the anisotropy quadrupole by the intervention of Thomson scattering in the cosmic medium. Solutions of the transfer equation for polarized radiation in the cosmological environment have been studied for a number of models; see refs. (24, 25), and also (26) for a short review. Theoretical predictions from perturbation models are often expressed in terms of angular power spectra, which are connected to the harmonic expansions

$$\Delta T = T_0 \sum_{l,m} a_{T,lm} Y_{lm}(\vartheta,\varphi),$$

$$Q \pm iU = T_0 \sum_{l,m} {}_{\pm 2}a_{P,lm}\ {}_{\pm 2}Y_{lm}(\vartheta,\varphi),$$

TABLE 2. Upper limits on CBR polarization degree.

Ref.	ν (GHz)	α	**Sky coverage**[a]	$\Pi_{\rm rms}$ ($\leq$)
(15)	4.0	15°	scattered	0.1
(16)	100–600	$1\overset{\circ}{.}5$–40°	GC	$(10\text{–}1)\times10^{-4}$
(17)	9.3	15°	$\delta = +40^\circ$	6×10^{-4}
(18)	33	15°	$\delta \in (-37^\circ, +63^\circ)$	6×10^{-5}
(19)	5.0	$18'$–$160'$	$\delta = +80^\circ$	$(1.4\text{–}0.4)\times10^{-4}$
(20)	26–36	$1\overset{\circ}{.}2$	NCP	1×10^{-5}
(21)	26–36	$1\overset{\circ}{.}4$	NCP	0.6×10^{-5}

[a] GC = Galactic Center, NCP = North Celestial Pole.

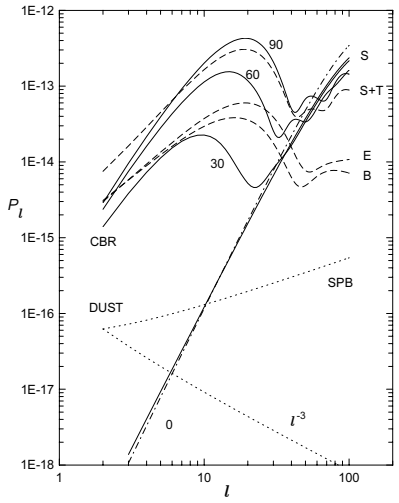

FIGURE 3. Polarization angular spectra from models of cosmic structure and Galactic dust emission. Full lines describe the CBR polarization in SCDM models with a baryon density $\Omega_{\rm b} = 0.03$ and a scale-invariant spectrum of scalar (S) waves, and are labelled by the corresponding values of $z_{\rm rh}$. Dashed lines refer to E- and B-parity contributions from tensor waves (labelled by E and B respectively), and to the total scalar-plus-tensor (S+T) polarization, normalized so as to get the same anisotropy quadrupole as in the scalar case. The dash-dotted curve considers a tilted $n = 1.2$ spectrum of scalar waves in the no-reheating model. Finally, the dotted curves describe the dust emission model of ref. (14) (SPB) and the l^{-3} law referring to foreground anisotropies.

involving the scalar and spin-weighted spherical harmonics, respectively denoted by $Y_{\ell m}$ and ${}_{\pm 2}Y_{\ell m}$ (27). The polarization spectrum is also altered substantially by gravitational lensing (28) and inhomogeneous reheating (29) for $l > 10^3$; on SPOrt angular scale, however, only spacetime perturbations are effective. Since the even (or electric) and odd (or magnetic) parities are separated through the linear combinations $a_{E,lm} = -\left({}_2a_{P,lm} + {}_{-2}a_{P,lm}\right)/2$ and $a_{B,lm} = i\left({}_2a_{P,lm} - {}_{-2}a_{P,lm}\right)/2$, four angular power spectra are usually provided,

$$C_{Xl} = \left\langle a^*_{X,lm} a_{X,lm} \right\rangle , \quad C_{Cl} = \left\langle a^*_{T,lm} a_{E,lm} \right\rangle , \tag{5}$$

with $X = T$, E and B. (Cross-correlations other than $C \equiv T \times E$ vanish identically.) The most obvious source of polarization, i.e. the density perturbation which originated the observed cosmic structure, only produce E-parity multipoles. E- and B-parity mixed fields are produced by all of the other sources, and unfortunately, by Galactic foregrounds (e.g., (14)).

The rms anisotropy and polarization at a given angular scale α can be estimated by $\Delta T_{\rm rms}(\alpha) \sim T_0\sqrt{T_{l^*}}$ and $P_{\rm rms}(\alpha) \sim T_0\sqrt{P_{l^*}}$, where

$$T_l = l(l+1)C_{Tl}/(2\pi), \quad P_l = l(l+1)C_{Pl}/(2\pi), \tag{6}$$

with $C_{Pl} = C_{El} + C_{Bl}$ and $l^* \sim 180^\circ/\alpha$, so that the quantities defined by Eq. (6) are usually plotted for power spectra. Examples are provided in Fig. 3. Full expressions of the polarization cross-correlation functions (including the autocorrelation $P_{\rm rms}(\alpha)$ as a simple case) in terms of the angular power spectra are given by Kamionkowsky et al. (30) and Ng and Liu (31).

Standard recombination models, where the CBR photons were last scattered at a redshift $z_{\rm rh} \approx 1000$, predict low levels of polarization at angular scales $\alpha \gtrsim 1^\circ$. Calculations performed in the SCDM model (the CDM model with the total density parameter $\Omega_0 = 1$ and the reduced Hubble constant $h = 1$) show that on a scale of 7° signals of order 0.05 μK are expected. Because of a significant increase in the P_l spectrum beyond the first temperature Doppler peak ($l \approx 200$), at scales below 1° the polarization-to-anisotropy ratio is of order 10%, so that we expect polarized signals as high as ~ 5 μK. The prospects for detection at larger scales are more favourable if the cosmic medium underwent a secondary ionization (reheating). In secondary ionization models polarization at angular scales $\alpha \gtrsim 1^\circ$ is produced at a new last-scattering surface placed

at a redshift $z_{\rm ls} \approx 100\Omega_0^{1/3}\,(0.025/X)^{2/3}$, with $X = x_{\rm e}\Omega_b h$ depending on the ionization degree $x_{\rm e}$, the baryon density parameter Ω_b and the reduced Hubble constant h, or at the reheating onset $z_{\rm rh}$ if $z_{\rm rh} < z_{\rm ls}$. Thus a characteristic angular scale (corresponding to the horizon size at $z_{\rm rh}$ or $z_{\rm ls}$) is introduced, which turns out to be in the degree range. The polarization spectrum is now peaked at such a scale, and suppressed at smaller scales.

The relevant parameters for secondary ionization models are the reheating redshift $z_{\rm rh}$, X, Ω_0, and the parameters of perturbation spectrum (the amplitude, the primordial spectral index n, and the shape factor $\Omega_0 h$ for CDM models). The most important combination of parameters is given by the approximate expression of the reheating optical depth for Thomson scattering

$$\tau_{\rm rh} \simeq 3.8 \times 10^{-2} X \Omega_0^{-1/2} z_{\rm rh}^{3/2}. \qquad (7)$$

The amplitude of the main peak in the angular spectrum P_l is roughly proportional to $\tau_{\rm rh}^2$ for $\tau_{\rm rh} \lesssim 1$, although it also depends on other parameters such as the perturbation spectral index; its position scales as $l \propto \tau_{\rm rh}^{1/3} X^{-1/3}$. These properties are clear in Figure 3 which gives angular spectra for a few CDM models. For $z_{\rm rh} = 90$ (corresponding to $\tau_{\rm rh} \simeq 0.5$) we find $T_0^2 P_{l,\max} \approx (1.8\ \mu{\rm K})^2$ at $l_{max} \simeq 20$. Slightly higher levels of polarization may be found with more favourable spectral shapes, in particular increasing the primordial index n. (This effect is more evident if models are normalized according to the power-spectrum quadrupole $Q_{\rm rms-PS}$.) However as we are going to discuss below, CBR signals larger than 1 μK, although they cannot be excluded, are not very likely to occur.

Experimental constraints and theoretical expectations for the reheating strength

While the Gunn–Peterson test on high-redshift objects implies $z_{\rm rh} \gtrsim 5$, it is more difficult to set stringent upper limits on the strength of reheating. One might expect that significant constraints on reheating should come from upper limits on the spectral distortions of CBR. However the COBE–FIRAS limit on the (generalized) Comptonization parameter, $y_{\rm C} < 1.5 \times 10^{-5}$, cannot exclude a large $z_{\rm rh}$; even no-recombination scenarios are possible if reionization is non-thermal (32). More significant constraints come from anisotropy data. The very existence of first Doppler peak implies $\tau_{\rm rh} \lesssim 1$, and a more significant result comes from the bulk of data on the harmonic spectrum. Fitting intermediate-scale anisotropy data with the standard SCDM model, de Bernardis et al. (33) give a best value $z_{\rm rh} \approx 20$, and an upper limit which depends on $\Omega_b h^2$ and can be as large as ~ 100 if $\Omega_b h^2 = 0.0075$.

This result can be used to set constraints on $\tau_{\rm rh}$ when combined with data on baryon density. Constraints on Ω_b are obviously given by the nucleosynthesis requirements. Olive (34) derives $\Omega_b h^2 = 0.006^{+0.009}_{-0.001}$ from ^{4}He and ^{7}Li data, but two mutually inconsistent results, $0.005 < \Omega_b h^2 < 0.014$ or $0.017 < \Omega_b h^2 < 0.022$ from Deuterium abundance, according as to whether one accepts a high (35) or low (36) D/H ratio. Fukugita et al. (37) compute a cosmic baryon budget from estimates of known contributions. From their results we derive the best estimate $\Omega_b h = 0.013 + 0.001 h^{1/2}$, and an upper limit $\Omega_b h = 0.025 + 0.003 h^{1/2}$. All of these constraints appear to be mutually consistent, with the exception of the Deuterium limit in the low-D/H case. From the cosmic baryon budget and the results of de Bernardis et al. (33), for $\Omega_0 = 1$ we can derive the upper limit $\tau_{\rm rh} \lesssim 0.7$, and a best estimate $\tau_{\rm rh} \sim 0.05$.

A low reheating optical depth is supported by explicit modelling of the ionizing mechanisms. Although a very small fraction of collapsing baryons would be enough to reionize the rest of the universe at early times, say at $z \sim 30$ or higher, it seems difficult to trigger the formation of stars or QSO black holes which should allow an early release of UV ionizing radiation. There was an early condensation of baryonic objects with $M \sim 10^5 M_\odot$ according to the CDM scenario, but an insufficient virialization temperature prevented further fragmentation or collapse of such condensed objects through H_2 cooling. Thus one must wait until objects with $M \gtrsim 10^8 M_\odot$ condense. Two different scenarios for the subsequent evolution of such objects are investigated by Haiman and Loeb (38,39). The first considers bursts of star formation with a universal mass function. The efficiency of star formation is calibrated by requiring that the resulting metallicity at $z \approx 3$ is roughly as observed, $Z \sim 10^{-2} Z_\odot$. The other scenario considers the production of low-luminosity, short-lifetime QSO's with a universal light curve. The background cosmology here (39) is not standard CDM, but the so-called "concordance" model, where the cosmological constant provides about 2/3 of the critical mass, but this makes no important difference. The basic requirement is now to match the observed luminosity function at $z \lesssim 5$. In both cases the growing number of expanding HII bubbles fills up the universe before $z \sim 10$, and the resulting optical depth is $\tau_{\rm rh} \simeq 0.05 \div 0.1$ for stars and $\simeq 0.05$ for QSO's.

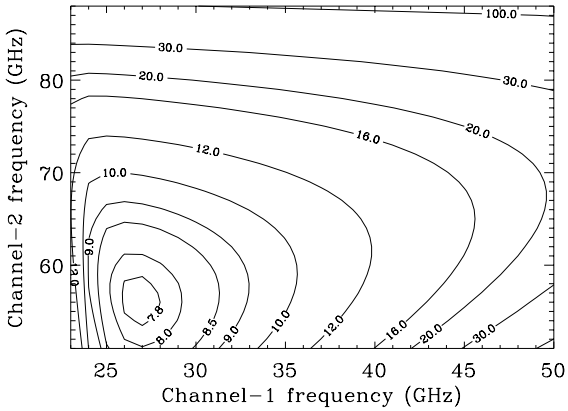

FIGURE 4. FDF isocontours in the (ν_1, ν_2) plane for fixed extremal frequencies 20 and 90 GHz. The minimum FDF is close to SPOrt intermediate frequencies.

We can thereby conclude that the polarized CBR signal at 7° is most likely to be found in the sub-μK range.

THE SEPARATION OF FOREGROUNDS

The separation of the contributions to polarized signals must be based on the different spectral and spatial behaviours of foregrounds and CBR. Multifrequency observations thereby play a fundamental role. We performed a preliminary analysis taking advantage of Dodelson's analytical formalism (40). This formalism allows us to estimate the experiment effective sensitivity for any signal component after subtracting other contributions on a single-pixel basis (or alternatively, on a single-mode basis after a spherical harmonic expansion). Let us consider an experiment measuring the total signal at frequencies ν_1, ν_2, ...ν_m and intended to extract the CBR and $n_{\rm f}$ foregrounds. Introducing the m-dimensional vectors $\mathbf{S}$, $\mathbf{N}$ and $\mathbf{F}^i$ for the detected signal, instrumental noise and foreground shapes respectively, we have $\mathbf{S} = \sum_{i=0}^{n_{\rm f}} s^i \mathbf{F}^i + \mathbf{N}$, with $i = 0$ denoting CBR, and the amplitudes s^i to be determined with the experiment. The problem is at which accuracy we can determine s^i when the noise is completely described by the auto- and cross-correlation coefficients $C_{jk} = \left\langle N_{\nu_j} N_{\nu_k} \right\rangle$. Focusing our attention on CBR and neglecting cosmic variance, the effective variance for one pixel or mode amplitude is given by

$$\sigma^2_{\rm cbr} = (FDF)^2 \left[\sigma^{(0)}\right]^2 + \sigma^2_{\rm shape}, \tag{8}$$

where the foreground degradation factor FDF describes the experiment sensitivity after removal of foregrounds with perfectly known spectral shapes, and $\sigma_{\rm shape}$ takes into account uncertainties in the spectral shapes. The computation of these parameters requires a matrix K^{ij} depending on $\mathbf{F}^i$ and noise cross-correlations (40). If all channels have equal and uncorrelated noise σ_{1ch}, then $\sigma^{(0)} = \sigma_{\rm 1ch}/\sqrt{\rm Nch}$ and $K^{ij} = \sum_{k,l} F^i_{\nu_k} F^j_{\nu_l}$. The final results provided by Dodelson are $FDF = \sqrt{(K^{-1})^{00}}$ and

$$\sigma^2_{\rm shape} = \left\{ \left(\sum_{i=1}^{n_{\rm f}} \mathbf{S}^i \right) \cdot \left[\sum_{j=0}^{n_{\rm f}} \left(K^{-1}\right)^{0j} \mathbf{F}^j \right] \right\}^2, \tag{9}$$

where $\mathbf{S}^i$ are the true foreground contributions to $\mathbf{S}$, whose spectral shapes may differ from the assumed $\mathbf{F}^i$. Systematic contributions to $\sigma_{\rm shape}$ may come from neglecting the contribution of some foreground component in the $\mathbf{F}^j$ summation in Eq. (9). The best effective sensitivity for CBR is reached by a proper balance of two contrasting effects, since increasing the number of fitted foregrounds makes $\sigma^2_{\rm shape}$ smaller but FDF larger.

The parameter FDF only depends on spectral shapes and frequency channels. The FDF level contours shown in Fig. 4 show that for the spectra given by Eqs. (1)–(4) the channel configuration of SPOrt is nearly optimal for the assigned range (20–90 GHz). Table 3 reports the values of the above parameters for different treatments of SPOrt output. Column 1 in the Table gives the number of channels used for the foreground

TABLE 3. The FDF and $\sigma_{\rm shape}$ for various foreground treatments.

Configuration	FF	Dust	FDF	$\sigma^{(1)}_{\rm shape}$	$\sigma^{(1)}_{\rm cbr}$	$\sigma^{(2)}_{\rm shape}$	$\sigma^{(2)}_{\rm cbr}$
4 (22–90)	Yes	Yes	8.80	0.00	2.52	0.00	2.52
4 (22–90)	No	Yes	2.76	0.77	1.10	0.64	1.02
4 (22–90)	No	No	1.38	0.61	0.73	0.25	0.47
3 (22–60)	No	No	1.54	0.64	0.80	0.17	0.51
3 (22–60)	Yes	No	3.60	0.24	1.16	0.24	1.16
4* (22–60)	No	No	1.37	0.59	0.70	0.18	0.42
4* (22–60)	Yes	No	3.21	0.24	0.92	0.24	0.92

fits and the frequency range. When the number of channels used is 3, the 90 GHz channel is not used; for the configuration labelled by 4*(22–60), which is not pertinent to the SPOrt present design, the computation assumes two 60-GHz channels. The second and third column specify whether free-free and dust emission are fitted. The results labelled by (1) (5-th and 6-th column) assume polarized intensities of 18 μK and 2 μK for synchrotron and free-free, respectively, at 30 GHz, and the assumed spectral slopes are $S = -3.2$ and $F = -2.15$; dust polarized emission is normalized to 1 μK at 200 GHz. For the results labelled by (2) we normalize synchrotron to 12 μK and dust to 0.15 μK at the same frequencies as above. The quantities $\sigma^{(1)}_{\rm cbr}$ and $\sigma^{(2)}_{\rm cbr}$, although they refer to the total sky coverage, are computed treating $\sigma_{\rm shape}$ as a systematic error. Clearly the best results are found when free-free and dust emission are not fitted (so that $\sigma^2_{\rm shape} \neq 0$). Using four channels we have $FDF = 1.38$ and $\sigma^{(1)}_{\rm shape} = 0.61$ μK, and using SPOrt total-coverage instrumental sensitivity from the above numbers we get $\sigma^{(1)}_{\rm cbr} = 0.73$ μK. For $\sigma^{(2)}_{\rm cbr}$ we can find some results even lower than 0.5 μK.

Slightly higher numbers are found using three channels for the synchrotron fit. The conclusion is that if dust emission is low, then the fourth channel adds little to the determination of CBR polarization in a single-pixel analysis; but if dust is important, it should probably not be included in a fitting together with synchrotron. A good strategy for data analysis may be the following, to use three channels up to 60 GHz for synchrotron and CBR polarized signals, and the 60 and 90 GHz channels for dust and CBR. With this approach it may be possible to investigate the roles of dust and synchrotron separately. In any case, differing from anisotropy measurements, it seems very difficult to measure free-free emission.

At this point, we can state that a conservative estimate of SPOrt full-sky sensitivity to CBR polarization, arising from a single-pixel analysis and taking into account a 50% efficiency factor, is around 0.5–0.7 μK, the uncertainty depending on the disturbance of free-free emission. However, considering free-free as a systematic effect in $\sigma_{\rm cbr}$ is too pessimistic. Going beyond the single-pixel analysis, we should exploit the spatial distribution of the signal. Spatial information is often exploited also using maps at other frequencies as templates, or for some kind of spatial cross-correlations. Basically we can work in real space or in terms of modes (for instance, using spherical harmonic expansions).

An important property of foregrounds is that they are more spatially correlated than CBR. This is well known for the temperature anisotropy: we have $C_{Tl} \propto l^{-3}$ for free-free (from COBE–DMR: see (7,8)) and dust (from IRAS (41)), while $C_{Tl} \propto [l(l+1)]^{-1}$ for the standard scale-invariant CBR spectrum. An important question however is, whether this is true for polarized foregrounds, too. Sethi et al. (14) found that for dust

$$T_0^2 C_{El} \simeq 8.9 \times 10^{-4} l^{-1.3} \ (\mu{\rm K})^2,$$
$$T_0^2 C_{Bl} \simeq 1.0 \times 10^{-3} l^{-1.4} \ (\mu{\rm K})^2,$$

where the smaller (less negative) exponents mean smaller spatial correlations than for anisotropies. However for CBR, too, the same inequality applies; as a result, polarized foregrounds seem to be more correlated than polarized CBR, as supported from the angular spectra reported in Fig. 3. Provided this conclusion can be generalized to the other foregrounds, a substantial improvement should come from a spatial or spectral analysis.

It is therefore reasonable to believe that the contribution of $\sigma_{\rm shape}$ can be significantly reduced, and we expect to be able to set $\sigma_{\rm cbr} \approx FDF\,\sigma^{(0)}$.

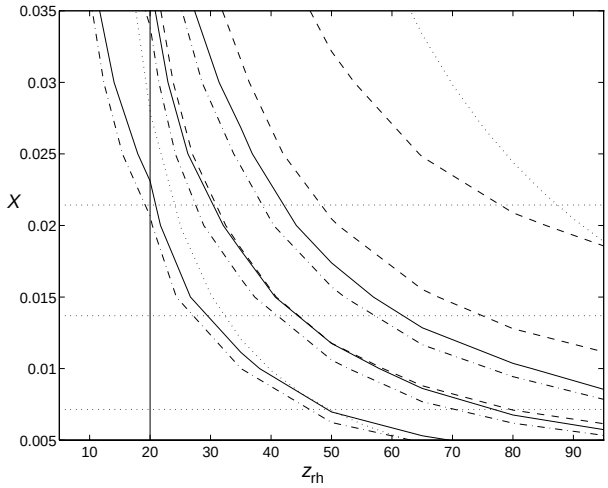

FIGURE 5. Polarization contours in the $(X, z_{\rm rh})$ plane corresponding to 7° squared fluctuations of 0.1, 0.25 and 0.5 μK^2. The contours refer to CDM models with $\Omega_0 = 0.9$ and 0.3 (full and dashed lines, respectively) and a CDM+texture model with $\Omega_0 = 0.7$ (dash-dotted). The dotted curves give the constant optical depth contours for $\Omega_0 = 0.9$ and $\tau_{\rm rh} = 0.7$ and 0.1. The horizontal dotted lines give the baryon density limits in ref. (34) and the best value in ref. (37). The vertical line gives the best fit result of de Bernardis et al. (33).

CONCLUSIONS

From the analysis of the previous section we can assume that SPOrt effective sensitivity to CBR polarization will be around 0.4 μK, (cfr. the 3-rd line in Table 3), or 0.5 μK including also the Galactic cut. This will allow us to probe a significant portion of parameter space for secondary ionization models. In order to check the validity of this conclusion, we performed extensive computations of secondary ionization models using routines of the SPOrtLIB library which is currently being built by the SPOrt collaboration. Some results are reported in Fig. 5, which provides polarization level contours in the $(z_{\rm rh}, X)$ plane for experiments with a 7° beamwidth. The contours represent predictions from some cosmic structure models (with a primordial spectral index $n = 1$ and normalized to COBE–DMR spectral amplitude $Q_{\rm rms-PS} = 18$ μK) computed for several values of Ω_0. For each value of Ω_0 (i.e., for each line style) the middle contour corresponds to the assumed full-sky sensitivity of 0.5 μK and thereby defines the region of the $(z_{\rm rh}, X)$ plane where, according to the assumed model of cosmic structure, the cosmological polarization is accessible to SPOrt; such a region extends towards the upper right corner of the Figure and is larger for $\Omega_0 \simeq 0.7$. The Figure also gives limits coming from the baryon density (for the assumed value $h = 0.7$) and some curves of constant $\tau_{\rm rh}$. Comparing the locations of the model contours with the $\tau_{\rm rh}$ curves it is clear that CBR polarization can be detected very easily for optical depths ~ 0.7, i.e. around the upper limit derived from de Bernardis et al. (33); for $\tau_{\rm rh} \sim 0.1$ SPOrt is likely to detect polarization around its sensitivity limit.

ACKNOWLEDGEMENTS

This work, as well as the SPOrt project, is supported by Agenzia Spaziale Italiana (ASI). The European Space Agency has supported SPOrt's A–B bridging phase under EPI industrial contracts. M.V.S. thanks the CentroVolta–LandauNetwork for financial support. I.A.S. thanks the Astronomy Dept. of the Bologna University and the ITeSRE/CNR for the support given to his participation to SPOrt activities.

REFERENCES

1. Bennet, C. L., Halpern, M., Hinshaw, G., Jarosik, N., Kogut, A., Limon, M., Meyer, S., Page, L., Spergel, D. N., Tucker, G., Wilkinson, D., Wollack, E., and Wright, E. L., "MAP–Microwave anisotropy probe", MAP Home

Page: http://map.gsfc.nasa.gov (1996).
2. Bersanelli, M., Bouchet, F. R., Efstathiou, G., Griffin, M., Lamarre, J. M., Mandolesi, N., Norgaard-Nielsen, H. U., Pace, O., Polny, J., Puget, J. L., Tauber, J., Vittorio, N., Volonté, S., "COBRAS/SAMBA−A mission dedicated to imaging the anisotropies of the cosmic microwave background", ESA Report D/SCI(96)3, PLANCK Home Page: http://astro.estec.esa.nl/SA-general/Projects/Cobras/cobras.html (1996).
3. Cortiglioni, S., Cecchini, S., Carretti, E., Orsini, M., Fabbri, R., et al., "The SPOrt project: an experimental overview", this volume (1998).
4. Brouw, W. N., and Spoelstra, T. A. Th., *Astron. Astrophys. Suppl.* **26**, 129–146 (1976).
5. Junkes, N., Fürst, E., and Reich, W., *Astron. Astrophys. Suppl.* **69**, 451–464 (1987).
6. Uyaniker, B., Fürst, E., Reich, W., Reich, P., and Wielebinski, R., "A 1.4 GHz radio continuum and polarization survey at medium Galactic latitudes: I. Observation and reduction technique", astro-ph/9807013, 1998.
7. Kogut, A., Banday, A. J., Bennet, C. L., Gorski, K. M., Hinshaw, G., and Reach, W. T., *Astrophys. J.* **460**, 1–9 (1996).
8. Kogut, A., Banday, A. J., Bennet, C. L., Gorski, K. M., Hinshaw, G., and Reach, W. T., *Astrophys. J.* **464**, L5–L8 (1996).
9. Davies, R. D., and Wilkinson, A., "Synchrotron emission from the Galaxy", astro-ph/9804208, 1998.
10. de Oliveira-Costa, A., Kogut, A., Devlin, M. J., Netterfield, C. B., Page, L. A., and Wollak, E. J., astro-ph/9702127 v2, 1997.
11. Keating, B., Timbie, P., Polnarev, A., and Steinberger, J., *Astrophys. J.* **495**, 580–596 (1998).
12. Wright, E. L., Mather, J. C., Bennet, C. L., Cheng, E. S., Shafer, R. A., et al., *Astrophys. J.* **381**, 200–209 (1991).
13. Draine, B. T., and Lazarian, A., *Astrophys. J.* **494**, L19 (1998).
14. Sethi, S.K., Prunet, S., and Bouchet, F.R., "Galactic dust polarized emission at high latitudes and CMB polarization", astro-ph/9803158, 1998.
15. Penzias, A. A., and Wilson, R. W., *Astrophys. J.* **142**, 419–421 (1965).
16. Caderni, N., Fabbri, R., Melchiorri, F., and Natale, V., *Phys. Rev. D* **17**, 1901–1907 (1978).
17. Nanos, G. P., *Astrophys. J.* **232**, 341–347 (1979).
18. Lubin, P. M., and Smoot, G. F., *Astrophys. J.* **245**, 1–17 (1981).
19. Partridge, R. B., Nowakowski, J., and Martin, H. M., *Nature* **331**, 146–147 (1988).
20. Wollack, E. J., Jarosik, N. C., Netterfield, C. B., Page, L., and Wilkinson, D., *Astrophys. J.* **419**, L49–L52 (1993).
21. Netterfield, C. B., Jarosik, N., Page, L., Wilkinson, D., and Wollack, E. J., *Astrophys. J.* **445**, L69–L72 (1995).
22. Sironi, G., Boella, G., Bonelli, G., Brunetti, L., Cavaliere, F., Gervasi, M., Giardino, G., and Passerini, A., *New Astron.* **3**, 1–13 (1998).
23. De Petris, M., "MITO Project", presented at International Conference on 3K Cosmology, Rome, 1998.
24. Sazhin, M.V., and Benitez, N., *Astron. Astrophys. Trans.*, **6**, 175 (1995).
25. Hu, W., Seljak, U., White, M., and Zaldarriaga, M., *Phys. Rev. D* **57**, 3290–3301 (1998).
26. Fabbri, R., "Polarization of the cosmic background radiation and secondary ionization of the cosmic medium", presented at International School of Space Physics, Course on 3K Cosmology, L' Aquila, 1998.
27. Zaldarriaga, M., "Fluctuations in the cosmic microwave background", PhD Thesis, Massachusetts Institute of Technology, astro-ph/9806122, 1998.
28. Zaldarriaga, M., and Seljak, U., "Gravitational lensing effect on the cosmic microwave background polarization", astro-ph/9803150, 1998.
29. Knox, L., Scoccimarro, R., and Dodelson, S., "The impact of inhomogeneous reionization on cosmic microwave background anisotropy", astro-ph/9805012, 1998.
30. Kamionkowski, M., Kosowsky, A., and Stebbins, A., *Phys. Rev. D* **55**, 7368–7388 (1997).
31. Ng, K. W., and Liu, G. C., "Correlation functions of CMB anisotropy and polarization", astro-ph/9710012 v2, 1998.
32. Tegmark, M., and Silk, J., *Astrophys. J.* **423**, 529–533 (1994).
33. de Bernardis, P., Balbi, A., de Gasperis, G., Melchiorri, A., and Vittorio, N., *Astrophys. J.* **480**, 1–5 (1997).
34. Olive, K.A., "Big bang nucleosynthesis", presented at Workshop on Theory and Phenomenology in Astroparticle and Underground Physics (TAUP97), Gran Sasso Laboratory, 1997.
35. Songaila, A., Cowie, L.L., Hogan, C., and Rugers, M., *Nature* **368**, 599–604 (1994).
36. Burles, S., and Tytler, D., *Astrophys. J.* **460**, 584–600 (1996).
37. Fukugita, M., Hogan, C.J., and Peebles, P.J.E., "The cosmic baryon budget", astro-ph/9712020, 1997.
38. Haiman, Z., and Loeb, A., *Astrophys. J.* **483**, 21–23 (1997).
39. Haiman, Z., and Loeb, A., "Observational signatures of the first Quasars", astro-ph/9710208, 1997.
40. Dodelson, S., *Astrophys. J.* **482**, 577–587 (1995).
41. Gautier, T. N., Boulanger, F., Perault, M., and Puget, J. L., *Astron. J.* **103**, 1313–1324 (1992)